ACE-2-derived Biomimetic Peptides for the Inhibition of Spike Protein of SARS-CoV-2

Saroj Kumar Panda[1$], Parth Sarthi Sen Gupta[1$], Satyaranjan Biswal,[1$] Abhik Kumar Ray,[1] and Malay Kumar Rana[1*]

[1]Department of Chemical Sciences, Indian Institute of Science Education and Research (IISER) Berhampur, 760010 Odisha.

Email: mrana@iiserbpr.ac.in

*Corresponding Author

[$]Authors contributed equally

Abstract:

SARS-CoV-2, a novel coronavirus causing overwhelming death and infection worldwide, has emerged as a pandemic. Compared to its predecessor SARS-CoV, SARS-CoV-2 is more infective for being highly contagious and exhibiting tighter binding with host angiotensin-converting enzyme 2 (hACE-2). The entry of the virus into host cells is mediated by the interaction of its spike protein with hACE-2. Thus, a peptide that has a resemblance to hACE-2 but can overpower the spike protein-hACE-2 interaction will be a potential therapeutic to contain this virus. The non-interacting residues in the receptor-binding domain of hACE-2 have been mutated to generate a library of 136 new peptides. Out of this library, docking and virtual screening discover seven peptides that can exert a stronger interaction with the spike protein than hACE-2. A peptide derived from simultaneous mutation of all the non-interacting residues of hACE-2 yields two-fold stronger interaction than hACE-2 and thus turns out here to be the best peptide-inhibitor of the novel coronavirus. The binding of the spike protein and the best peptide-inhibitor with hACE-2 is explored further by molecular dynamics, free energy, and principal component analysis to demonstrate its efficacy. Further, the inhibition assay study with the best peptide inhibitor is in progress.

Keywords: SARS-CoV-2, hACE-2, COVID-19, Peptide inhibitor, Molecular dynamics

Graphical abstract

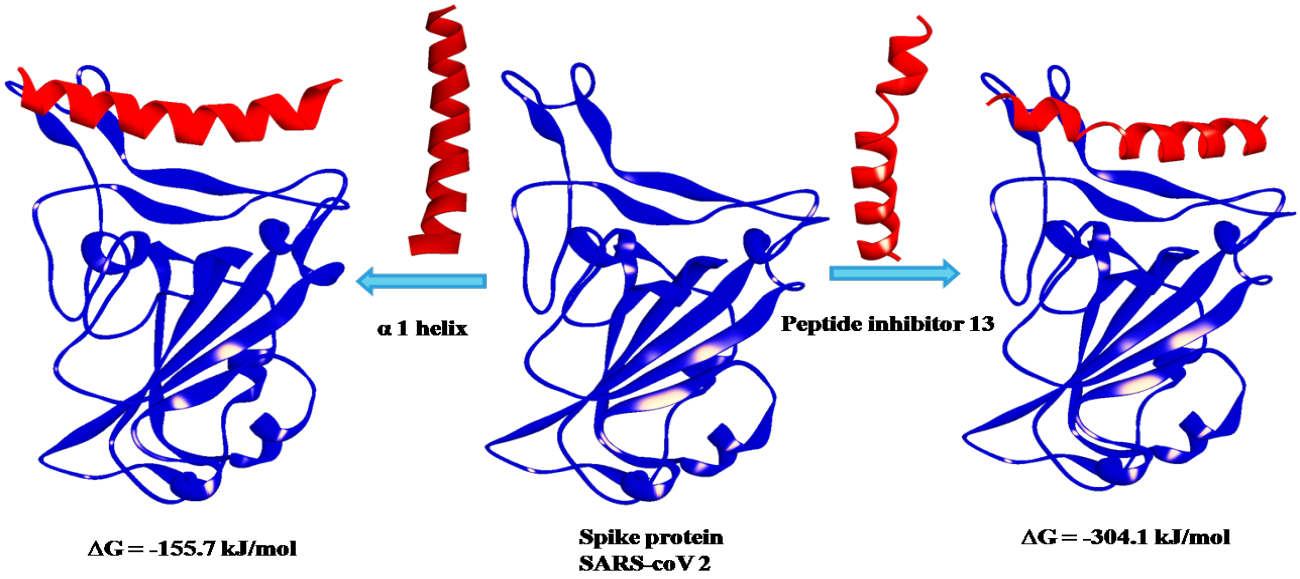

1. Introduction

A current death toll and infected cases surged into millions is caused by the novel coronavirus COVID-19, engendering an unprecedented global containment. While no approved cure is available so far for the severe acute respiratory syndrome coronavirus 2 (SARS-CoV-2), the COVID-19 pandemic has put health, lives, economies, societal relations, and humanitarian at risk[1]. Based on epidemiological data, unlike its predecessors, SARS-CoV-2 is highly contagious in humans, spreading through close contact and respiratory droplets, reasoned for the occurrence of this pandemic[2,3]. It targets the lower respiratory system to induce viral pneumonia similar to earlier SARS-CoV and MERS-CoV.[4,5]

SARS-CoV-2 is a beta-coronavirus and belongs to Coronavirinae subfamily of Coronaviridae genera, consisting of a single-stranded positive sense RNA genome with nucleocapsid protein, covered by a lipid bilayer membrane containing hemagglutinin-esterase dimer, envelope, and membrane proteins and spangled with spikes of glycoproteins, which give a coronary appearance.[6] Based on the sequence alignment and homology analysis, SARS-CoV and SARS-CoV-2 share a strongly conserved receptor-binding domain (RBD). There are 14 residues in the RBD region of SARS-CoV-2 which actively participate in the interaction with hACE-2. Out of 14 residues, 8 amino acid residues are common between both viruses, Tyr449/Tyr436, Tyr453/Tyr440, Asn487/Asn473, Tyr489/Tyr475, Gly496/Gly482, Thr500/Thr486, Gly502/Gly488 and

Tyr505/Tyr491 of SARS-CoV-2/SARS-CoV. Five residues, albeit not common structurally, render similar biochemical properties in both, Leu455/Tyr442, Phe456/Leu443, Phe486/Leu472, Gln493/Asn479 and Asn501/Thr487 of SARS-CoV-2/SARS-CoV. The remaining one amino acid differs - Gln498/Tyr484 (SARS-CoV-2/SARS-CoV).[7-9] The surface plasmon resonance showed that the binding affinity of SARS-CoV-2 spike protein to hACE-2 is around 10−20 times greater than that of SARS-CoV spike protein,[10-14] making it more harmful than the latter. This is attributed to several mutations in the SARS-CoV-2 RBD region and a more compact conformation of hACE-2-binding ridge, which stabilize two virus-binding hotspots of hACE-2 more.[8] In passing, the structural analysis clearly indicates that a convergent evolution between the SARS-CoV-2 and SARS-CoV RBDs has boosted the ACE-2 binding.[15-17] Thus, the interaction between the viral spike protein and hACE-2 on the host cell surface is of great importance to initiate infection. The host ACE-2 interacts with the RBD domain of the spike protein, mainly via α-1 helix, as most of the interactions are from α-1 helix of hACE-2.[9] Design of new peptide inhibitors mimicking α-1 helix and having significantly higher binding affinity to RBD than α-1 helix is a very important and an unexplored avenue to discover potent therapeutics of the novel coronavirus by preventing hACE-2-RBD interactions. Despite cumulative efforts at all corners of the globe, no confirmed effective treatment is yet ready for COVID-19.

In this study, a library of 136 biomimetic peptide inhibitors against SARS-CoV-2 was designed, docked, and simulated, which mimic hACE-2 but incorporate necessary mutated components for the non-interacting residues in hACE-2's virus-binding domain, based on the recently published crystal structure (PDB code: 6M0J), to enhance interaction with the spike protein. The α-1 helix of hACE-2 was taken as a reference peptide for designing the peptide library, which contains key amino acids that take part in the interaction with RBD of the spike protein. The α-1-helix-derived designed biomimetic peptide-inhibitors (**Figure 1**) each of 23 residues long had shown greater interaction than α-1 helix of hACE-2. All the inhibitors are structurally stable and have relatively small molecular weights. Out of them, seven peptide inhibitors manifest greater binding affinity to the spike protein than α-1 helix. Stability and interaction of the best-screened peptide inhibitor complexed with the spike protein were validated using molecular dynamics (MD) simulation and MMPBSA binding free energy calculation. Compared to α-1 helix-spike protein, there is greater stability of the complex of the designed best peptide implying it is a potent inhibitor of the spike protein which can rupture the hACE-2-spike interaction.

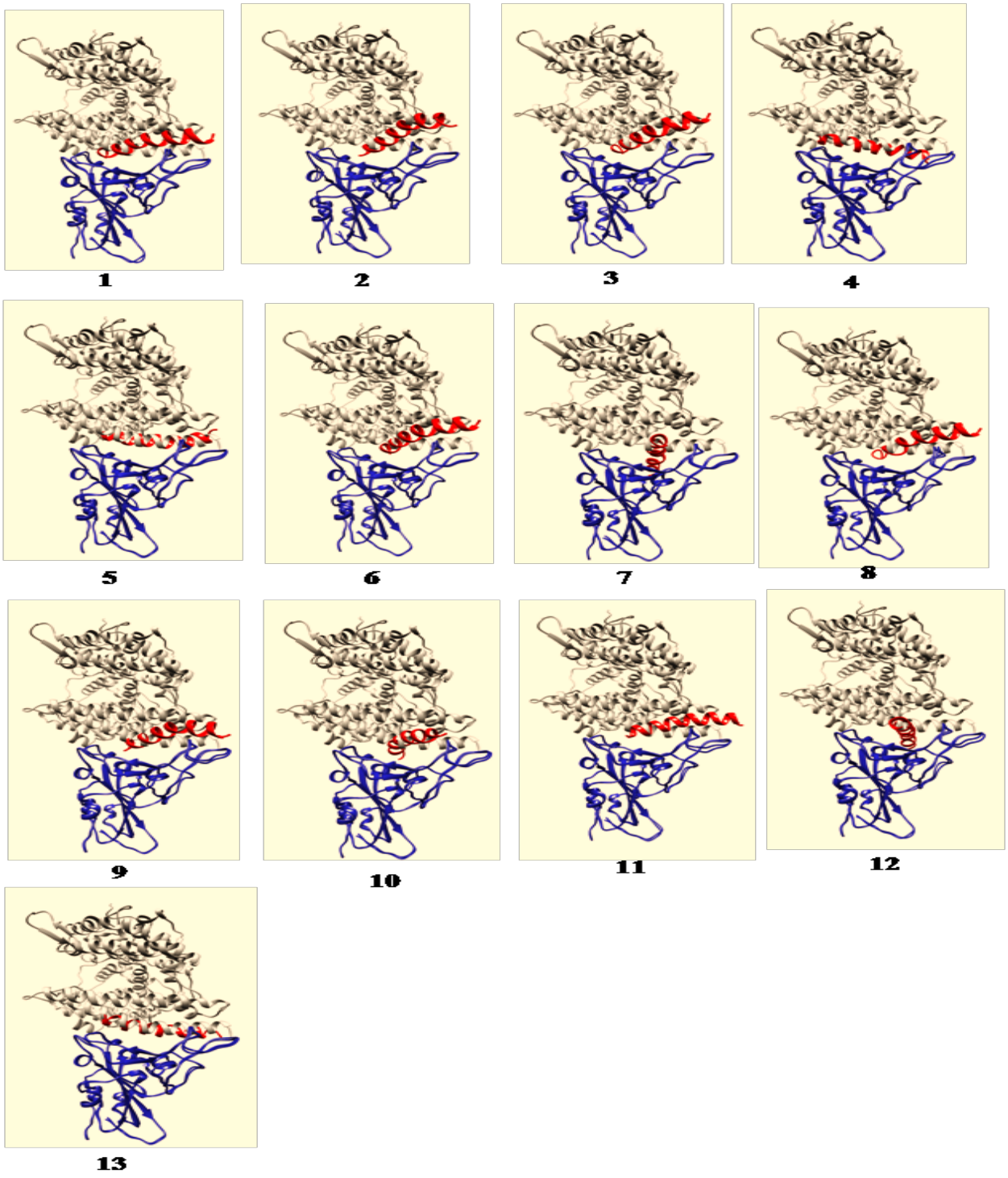

Figure 1: **The binding poses of the top 13 designed biomimetic peptide inhibitors in the RBD region of the spike protein. Peptides, Spike protein and hACE-2 are shown in red, blue, and grey colors, respectively.**

2. Materials and methods:

2.1 Designing peptide-inhibitor library

To construct a peptide library, the crystal structure of hACE-2 bound to the spike protein with PDB ID: 6M0J was considered as a reference in the present study.[18] Between the RBD region of the spike protein and hACE-2, there exist a total of fifteen interactions, which include 13 hydrogen bonds (h-bond) and 2 salt-bridge interactions. The interacting residues pertaining to the host receptor hACE-2 are ASP30, TYR41, GLN42, TYR83, ASN30, ASP38, GLN24, GLU35, GLU37, TYR325, GLU329, ASN330, and LYS353. Most of the interaction is from the hACE-2 α-1 helix domain because of which it was taken here as a template to design new peptide inhibitors. [19-21] Having a greater affinity of the designed biomimetic peptides to RBD may warrant to prevent hACE-2-RBD interactions. To make highly specific and stable peptide binders, the α-1 helix of hACE-2 consisting of 23 amino acids located between 21-44 residues was taken. Out of these 23 amino acid residues, ASP30, GLN24, GLN42, TYR41, ASP38, GLU35, GLU37, and LYS31 are seen presently interacting with the spike protein receptor binding domain. To design a peptide library, the non-interacting residues of α-1 helix were mutated with all possible combinations to generate a total of 136 biomimetic peptides using the mutator plugin of VMD. The mutated peptides thus formed are energy minimized applying the amber99sb force field in UCSF Chimera.

2.2 Molecular docking and interaction analysis

All the designed 136 mutated peptides and α-1 helix (reference peptide) of hACE-2 were docked in the active site of the spike protein by using the High Ambiguity Driven protein-protein Docking (HADDOCK) server. [22] HADDOCK facilitates information-driven, flexible docking for modeling of bimolecular complexes. With a wide capability to deal with protein-protein, protein-nucleic acids, protein-ligand, etc., docking, HADDOCK distinguishably differs from *ab initio* docking methods by encoding information from identified or predicted protein interfaces in ambiguous interaction restraints (AIRs) to drive the docking process. The active-site residues 403, 417, 446, 449, 453, 487, 489, 493, 500, and 505 from the receptor-binding region of the spike protein were selected owing to participating in the interaction with hACE-2. The best docking poses which have the highest negative HADDOCK scores were filtered out. As a consequence, the best 13 peptides resulted out of a mutation of 12 different residues were identified among the top HADDOCK scores. The sequences of 12 high scoring mutated peptides were given in **Table 1** where their best

docking poses inevitably show good interaction with the spike protein. Finally, the best peptide (No. 13) was obtained by mutating all 12 non-interacting residues of α-1 helix simultaneously with the best scoring residues from the 12 initially screened out peptides. **Table 2** presents the docking scores along with interacting residues of α-1 helix; the peptide-inhibitor 13 with the best docking score and α-1 helix bound to the spike binding domain were selected for molecular dynamic (MD) simulation and binding free energy calculation.

2.3 MD simulation and Binding free energy calculation

MD simulations were run for the spike protein bound to α-1 helix and the mutated peptide no. 13 using GROMACS 5.1.4 for 50 ns.[23-26] The AMBER ff99SB force field was used for the proteins.[21] The respective docked complexes were engrossed in a cubical box of simple point charge (SPC) water molecules. The complexes were neutralized by adding an appropriate number of Na^+ and Cl^- ions. To get rid of short-range bad contacts, energy minimization was performed using the steepest descent method for 50,000 steps. Then the systems were subjected to 50 ns MD simulation runs at 298 K temperature and 1 bar pressure, using 0.002 ps time step and the Berendsen thermostat. Finally, the root-mean-square deviation (RMSD), root-mean-square fluctuation (RMSF), the radius of gyration (Rg), essential dynamics, and the average structure after MD simulations were evaluated to investigate conformational changes and the stability of the peptide inhibitors bound to the spike protein.

Subsequently, binding free energies of the spike bound the best peptide inhibitor and α-1 helix complexes was calculated on the 50 ns of MD simulation trajectories taking 5000 configuration snapshots. The total binding free energy and its components: electrostatic energy, polar and apolar solvation energies, and the van der Waals energy were calculated using the MM-PBSA method executed by the g_mmpbsa tool.[27,28] The per-residue energy contribution of the complexes was also estimated.

3. Results and discussion

2.3 Peptide library

A single-point mutation and simultaneous mutation of non-interacting residues of hACE-2 in the active region, namely for GLU22, GLU23, ALA25, LYS26, THR27, PHE28, LEU29, PHE32, ASN33, ALA36, LEU39, and PHE40, at multiple locations have been carried out to form a 136-

peptide library. The exhaustive list of the top 13 peptide sequences filtered out can be found in **Table 1**. All these mutations are shown in red color in the peptide sequences presented in **Table 1**.

Table 1: The sequences of the top 13 peptide-inhibitors derived from the mutation of α-1 helix of hACE-2 are presented. Mutated residues are marked in red color.

Biomimetic peptide inhibitors	Sequences of peptide
α-1 helix (reference)	IEEQAKTFLDKFNHEAEDLFYQSS
1	IDEQAKTFLDKFNHEAEDLFYQSS
2	IEWQAKTFLDKFNHEAEDLFYQSS
3	IEEQFKTFLDKFNHEAEDLFYQSS
4	IEEQAWTFLDKFNHEAEDLFYQSS
5	IEEQAKFFLDKFNHEAEDLFYQSS
6	IEEQAKTHLDKFNHEAEDLFYQSS
7	IEEQAKTFYDKFNHEAEDLFYQSS
8	IEEQAKTFLDKWNHEAEDLFYQSS
9	IEEQAKTFLDKFDHEAEDLFYQSS
10	IEEQAKTFLDKFNHEWEDLFYQSS
11	IEEQAKTFLDKFNHEAEDWFYQSS
12	IEEQAKTFLDKFNHEAEDLWYQSS
13	IDWQFWFHYDKWDHEWEDEWYQSS

2.4 Molecular docking and interaction analysis

The docking poses of the top 13 mutated peptide inhibitors are shown in **Figure 1**. The docking scores, non-interacting residues, and the h-bond interaction are reported in **Table 2** for the same

peptides. There are 7 peptides which have higher docking scores, ranging between -118.9 ± 3.1 to -150 ± 3.7, than the reference peptide α-1 helix of hACE-2 (-118.5±5.5). Among all, the peptide inhibitor 13 exhibits the highest docking score of -150 ± 3.7 along with a greater number of interactions with the spike RBD (**Table 2**). The interacting residues of peptide 13 within a 3.10 Å distance of the spike RBD are ARG403 (2), ARG417 (2), TYR421, TYR449, TYR453, GLN493, TYR505, THR500, and ALA475.

Table 2: The docking scores and h-bond interaction of the best-screened 13 mutated peptide inhibitors.

Peptide inhibitors	**Non interacting residues**	**Mutation**	**Docking scores**	**H-bond interaction within 4 Å**
α-1 helix (reference)	GLU 22, GLU 23, ALA 25, LYS 26, THR 27, PHE 28, LEU 29, PHE32, ASN33, ALA36, LEU39, PHE40	—	-118.5±5.5	LYS417, GLY446, TYR449(2), ASN487, THR500, TYR505
1	GLU 22	ASP	-111.4 ±2.4	GLU484, PHE486, GLN493, GLN498(2), THR500, ASN501 (2), TYR505, GLY496, GLY446 (2), GLY485
2	GLU 23	TRP	-123.1 ± 7.7	ARG403(2), TYR449, ASN487(2), TYR489, TYR505
3	ALA 25	PHE	-104.5 ± 1.4	GLU484, GLN498, ASN501, TYR505

4	LYS 26	TRP	-132.4 ± 6.3	ARG403(2), LYS417(2), TYR449, THR500, TYR505,
5	THR 27	PHE	-125.2 ± 2.8	LYS417, TYR473, ASN487, TYR489, GLN493, THR500(2), TYR505(2)
6	PHE 28	HIS	-99.8 ± 1.8	GLU484, TYR453, TYR505(2), GLN493, PHE490
7	LEU 29	TYR	-127.6± 23.6	ARG403, LYS417(2), ARG408, GLN414, THR415, LYS417, TYR505, THR415, TYR421, GLU484
8	PHE32	TRP	-119.4 ± 3.3	GLU484(2), TYR453, PHE486, GLN493, ASN501, GLY496, GLY485, CYS488
9	ASN33	ASP	-102.3 ± 2.9	ARG403(2), PHE486, ASN487, TYR489, TYR505, TYR449, GLN498
10	ALA36	TRP	-116.8 ± 6.0	ARG403, ARG408, TYR505, GLN493, GLY485, GLU484, TYR453

11	LEU39	TRP	-118.9 ± 3.1	ARG403, TYR453, ASN487, TYR489, GLY496, TYR453
12	PHE40	TRP	-111.4± 0.8	THR415, LYS417, TYR489, GLN493, TYR505, GLY485
13	GLU 22, GLU 23, ALA 25, LYS 26, THR 27, PHE 28, LEU 29, PHE32, ASN33, ALA36, LEU39, PHE40	Above 12 mutations (combined)	**-150 ± 3.7**	ARG403 (2), ARG417 (2), TYR421, TYR449, TYR453, GLN493, TYR505, THR500 and ALA475

Apart from a significantly lower binding energy than that for α-1 helix of hACE-2, the designed peptide 13 has 11 h-bonds and 4 salt-bridges (ARG403(2), LYS417(2)) in comparison to the 7 h-bonds and 2 salt-bridges (LYS417, ARG403) of the former. The closer proximity of 3.10 Å indeed reflects a very strong interaction and inhibition capability of the peptide 13 towards the virus spike protein.

2.5 MD simulation and binding free energy calculation

MD simulations were performed to obtain deeper insights into the stability and dynamic properties of the spike-bound α-1 helix and the designed best-screened peptide inhibitor. This is quite useful to assess how the natural motions of proteins or peptides can affect the protein–peptide interactions, the stability of the bound complexes, and their conformations due to binding. After the MD simulation, for comparison, the initial and final structures of α-1 helix and the designed best peptide inhibitor 13 were superimposed in **Figure 2**.

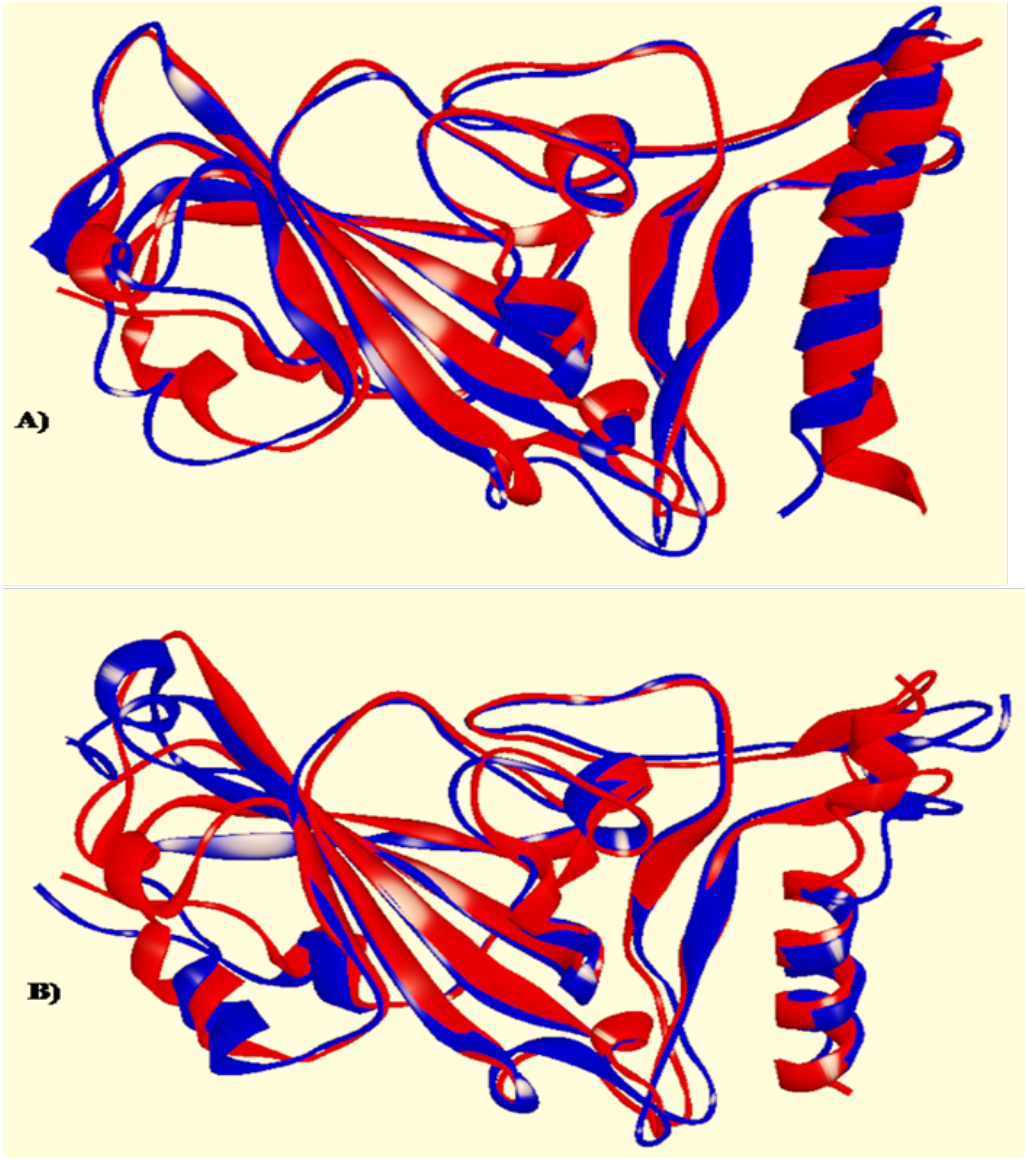

Figure 2: Superimposition of the initial (red) and final structure after 50 ns MD (blue) of the spike protein bound to (A) α-1 helix and (B) the designed peptide inhibitor 13.

Figures 3A and B represent the RMSD plots of the spike protein complexes of α-1 helix and the best-screened peptide inhibitor 13, respectively. Although both the spike protein and α-1 helix do not show a significant change in their respective RMSD values, the RMSD of both the spike protein and the peptide inhibitor 13, however, increases, an indication of a strong interaction

interplaying between them leading to a substantial conformational change before getting locked into a stable bonded conformation. Such conformational changes are more evident in the superimposed initial and final (after 50 ns MD) structures of the spike bound peptide inhibitor 13 complex (**Figure 2B**). In contrary, one finds a very little change for the α-1 helix-spike complex (**Figure 2A**) for no remarkable interaction compared to the previous complex.

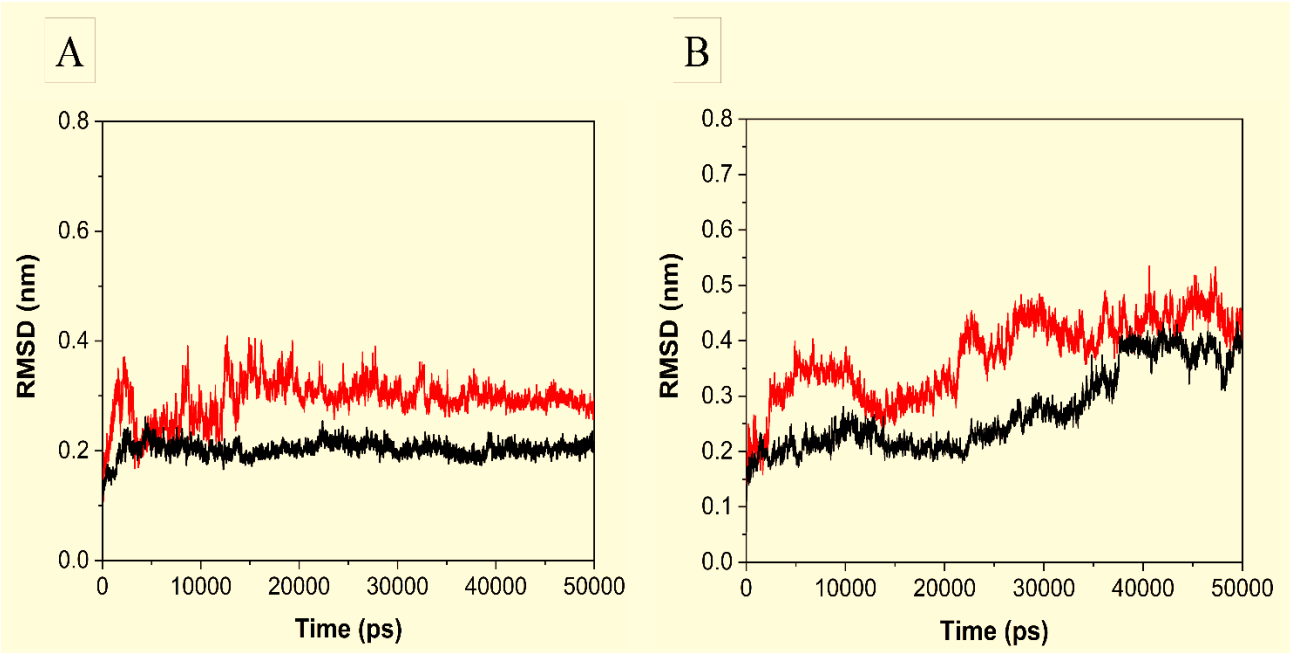

Figure 3: The **RMSD of the (A) spike protein (black) bound α-1 helix (red) and (B) spike protein (black) bound the best peptide inhibitor 13 (red) plotted as a function of simulation time.**

Figures 4A and B show the RMSF of Cα atoms of both the complexes. In **Figure 4A**, a similar fluctuation in the regions 21-34 and 38-44 amino acid residues between both the peptides bound to the spike protein could be observed. A stake that appeared for residues 35-37 in the RMSF plot of the peptide inhibitor 13 is attributed to the presence of loops, please see the peptide snapshot in **Figure 4A**. The patterns of fluctuations in the RMSF plots (**Figure 4B**) of the Cα atoms of the spike protein bound to both the inhibitors are very similar to that for the peptides. A more fluctuating region lies between 380-390 residues in the spike protein bound to the peptide inhibitor 13. Again, such fluctuation arises not from the active region, but from the loop region as shown in the snapshot in **Figure 4B**. All the residues 400-505 in the active region rather show less fluctuation. As far as the active site is concerned, both the peptide inhibitors are stable when bound

to the spike binding domain as the RMSF indicates. Loop fluctuation can bring in more non-bonded interaction between the respective peptide and the spike protein.

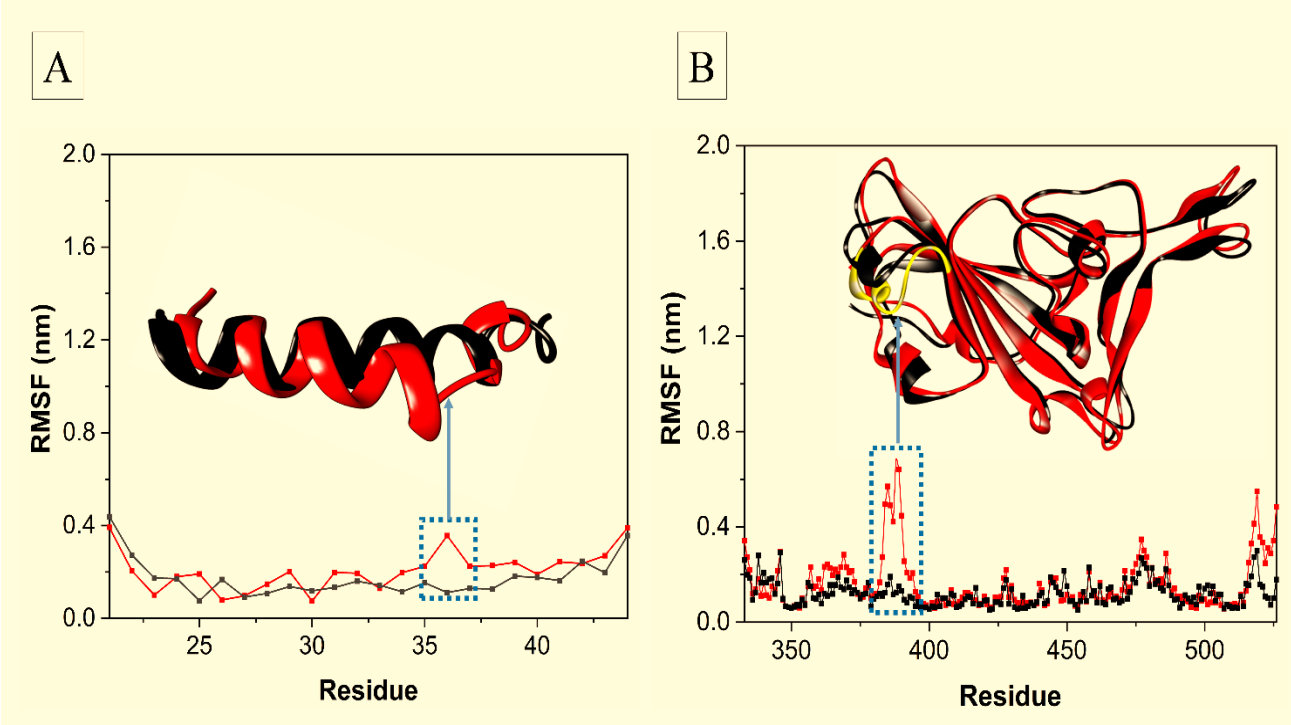

Figure 4: The RMSF of amino acid residues in (A) α-1 helix (black) and the designed peptide inhibitor 13 (red) and (B) the spike protein bound to α-1 helix (black) and to the designed peptide inhibitor 13 (red) is plotted as a function of simulation time. The fluctuating residues (380 to 390) of the spike protein are displayed in yellow color.

The **radius of gyration** (R_g), which is a mass-weighted root-mean-square distance for a collection of atoms from their common center of mass, describes the level of compaction depicting the overall dimension of protein. Plots of R_g in **Figures 5A and B,** respectively, for the α-1 helix and the designed peptide 13 bound spike protein complexes show that in the former complex, the individual peptide/protein is more compact than that for the latter because of the lower R_g values. This suggests less interaction prevailing in α-1 helix-spike than the peptide 13-spike.

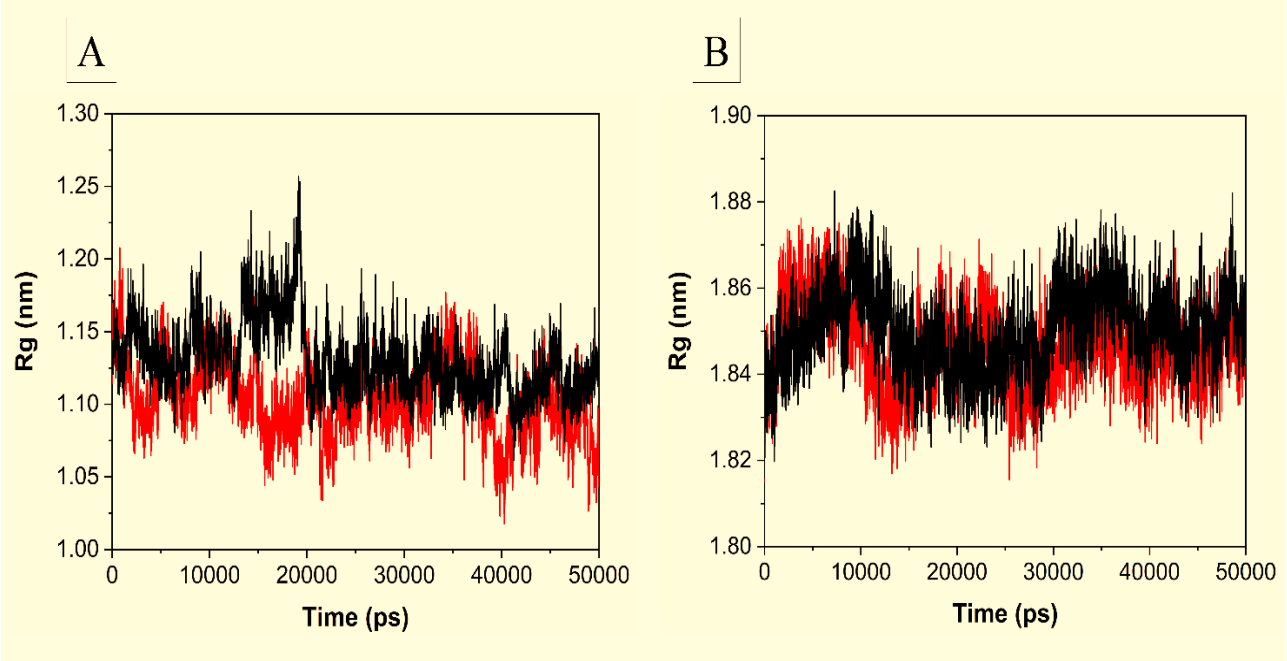

Figure 5: The radius of gyration (R_g) of (A) the spike protein (black) bound to α-1 helix (red) and (B) the spike protein (black) bound to the designed peptide inhibitor 13 (red) is plotted as function of simulation.

The binding free energy provides the binding strength of a peptide and hence its potential to inhibit the hACE-2 protein, which is given in **Table 3**. Compared to α-1 helix which has -155.8 ± 25.3 kJ/mol binding free energy, the peptide inhibitor 13 displays almost twice as small as the value of the former (-304.1 ± 30.6 kJ/mol) confirming a very strong interaction with the receptor binding domain of the spike protein. This reinforces that the mutant peptide 13 is indeed a powerful inhibitor of the spike protein, thus can potentially shield the attack of the virus and consequently its entry into host cells. For better insight, the contributions from active residues in the peptides bound to the spike protein are provided in **Table S1 (supporting information)**.

Table 3: **The binding free energy and contributions of the van der Waals, electrostatic, polar solvation, and apolar solvation energies to it (kJ/mol) in the α-1 helix and peptide inhibitor 13 bound spike protein complexes.**

Peptide inhibitor bound spike protein complexes	Van der Waals energy	Electrostatic energy	Polar solvation energy	Apolar solvation energy	Binding free energy

α-1 helix	-72.4 ± 13.6	-295.8 ± 42.6	221.7 ± 37.6	-10.7 ± 2.0	-155.8 ± 25.3
Peptide inhibitor 13	-144.2 ± 20.0	-579.7 ± 71.3	438.7 ± 58.2	-19.1 ± 2.6	**-304.1 ± 30.6**

The per-residue binding free energy plot provided in **Figure 6** highlights that most of the mutated residues show favorable binding energy in comparison to the wild-type. The E22D, K26W, N33D, E39L, and F42W mutations display larger contributions to binding to the spike protein. Apart from these, some amino acid residues contributing higher energy than α-1 helix are D30, E35, E37, and D38.

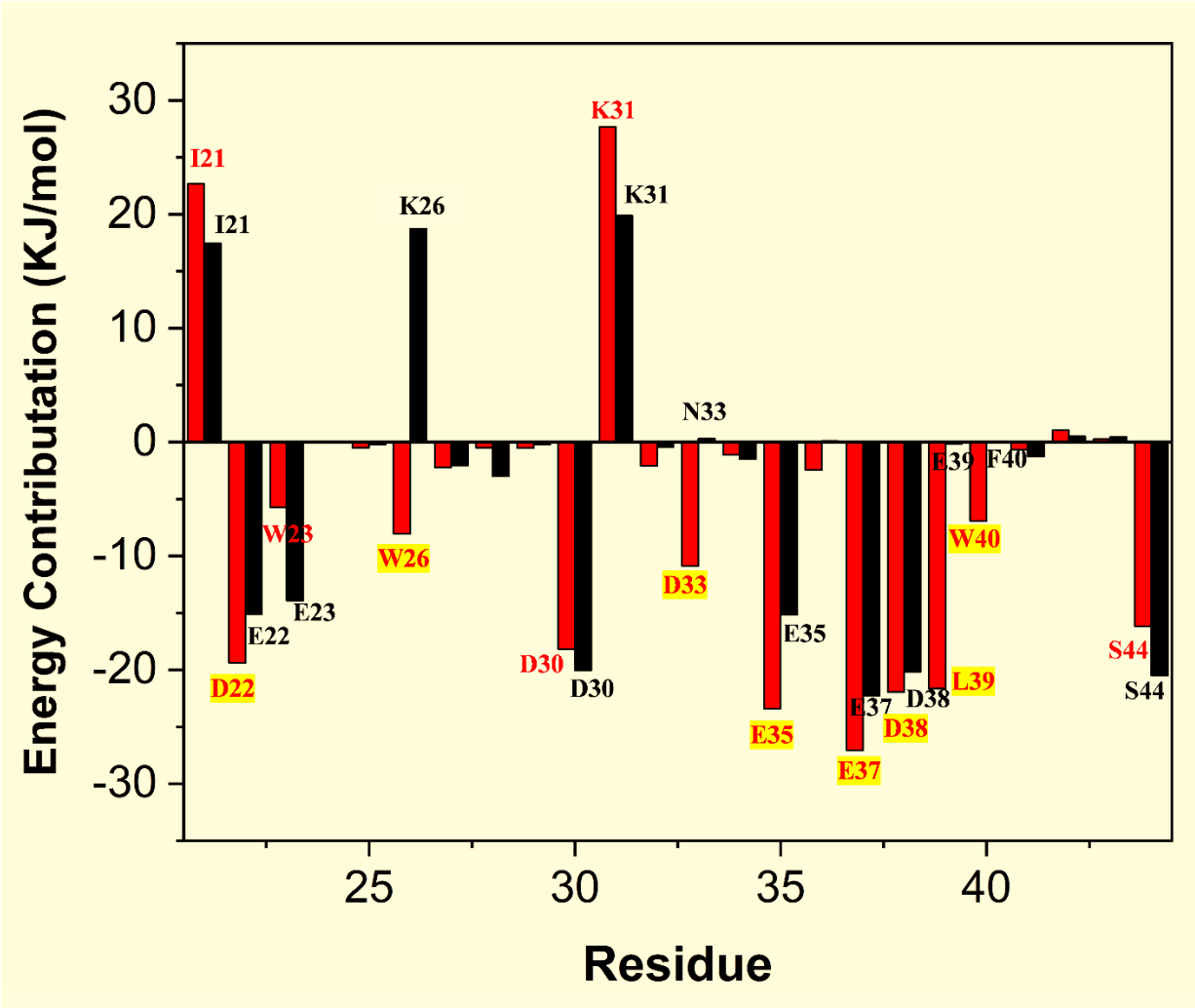

Figure 6: The per-residue contribution plot for the designed peptide inhibitor 13 (red) and α-1 helix (black) bound to the spike protein. The residues highlighted in yellow color are the major contributing residues of the designed biomimetic peptide 13.

Principal component analysis (PCA) or essential dynamics (ED) is used to portray the directions of principal motions by a set of eigenvectors (EV) called the principal or essential modes. PCA is a linear transformation that extracts important spatial data (e.g., the Cartesian coordinates for the atomic displacements in MD trajectory) using a covariance matrix, which describe the accessible degrees of freedom (DOF) of a protein. **Figure 7** presents the PCA results in the 2D plot**.** Taken the first two PCs into consideration, simulation results reveal a higher subspace dimension for the α-1 helix-spike protein complex.

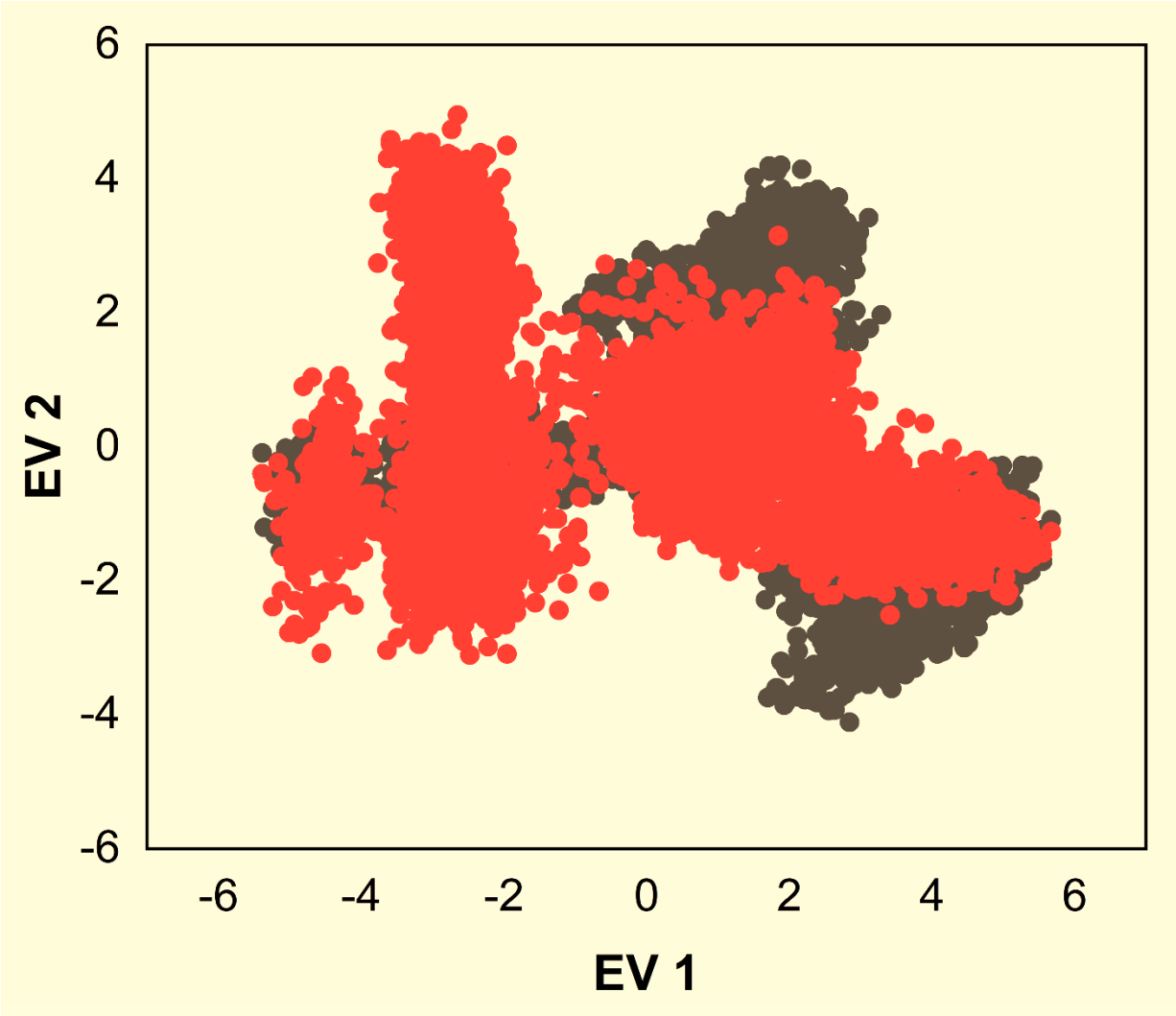

Figure 7: 2D scatter plots of α-1 helix (black) and the designed peptide inhibitor 13 (red), projecting the motion in phase space for the first two principle components (EV1 and EV2 are eigenvectors 1 and 2, respectively).

On the contrary, the designed peptide 13-spike protein complex covers relatively a smaller subspace. In the 2D projection plots, the α-1 helix-spike protein complex shows higher trace values of the covariance matrix than that for the peptide 13-spike complex. The overall analysis again suggests that the peptide inhibitor-spike protein complex has greater stability/interaction than the α-1 helix-spike protein complex.

4. Conclusion

To hinder the fusion of the spike protein with hACE-2, 136 peptide-inhibitors of hACE-2 analogs have been designed by sequential and simultaneous mutations of the non-interacting residues in the α-1 helix of hACE-2. Seven peptides that have stronger interaction with the spike protein than α 1 helix of hACE-2. The affinity of the best screened peptide inhibitor, derived from mutating all the non-interacting residues, to the spike protein is almost twice that of hACE-2. Such a strong affinity can misguide the spike protein from attaching to hACE-2 preventing viral entry and infection into host cells. Besides, the designed peptides having docking scores lower than -123 could be also a promising inhibitor. Post-molecular dynamics analysis, e.g., RMSD, RMSF, Rg, binding free energy, number of h-bonds and salt bridges, and PCA clearly demonstrate tighter binding of the best-screened peptide with the Spike protein compared to hACE-2. Finally, the best peptide inhibitor identified herein definitely has a greater chance to serve as a potential therapeutic of SARS-CoV-2 and can be worthy of further experimental investigation that is under consideration.

Acknowledgements

The authors acknowledge IISER Berhampur for computational support. P.S.S.G also sincerely acknowledges IISER Berhampur for providing him the Institute Postdoc Fellowship to carry out this work.

Conflict of interest

The authors report no conflicts of interest.

References

1. Wang, Chen, Peter W. Horby, Frederick G. Hayden, and George F. Gao. "A novel coronavirus outbreak of global health concern." *The Lancet* 395, no. 10223 (2020): 470-473.
2. Gorbalenya, A. E. et al. The species severe acute respiratory syndrome-related coronavirus: classifying 2019-nCoV and naming it SARS-CoV-2. Nature Microbiology 2020, DOI: 10.1038/s41564-020-0695-z
3. Kupferschmidt, K.; Cohen, J. Will novel virus go pandemic or be contained? Science 2020, 367 (6478), 610-611
4. Su, S.; Wong, G.; Shi, W.; Liu, J.; Lai, A. C.K.; Zhou, J.; Liu, W.; Bi, Y.; Gao, G. F. Epidemiology, genetic recombination, and pathogenesis of coronaviruses. Trends Microbiol. 2016, 24 (6), 490-502.
5. Zhu, N.; Zhang, D.; Wang, W.; Li, X.; Yang, B.; Song, J.; Zhao, X.; Huang, B.; Shi, W.; Lu, R.; Niu, P.; Zhan, F.; Ma, X.; Wang, D.; Xu, W.; Wu, G.; Gao, G. F.; Tan, W. A novel coronavirus from patients with pneumonia in China, 2019. N. Engl. J. Med. 2020, 382 (8), 727-733.
6. Anthony, S. J.; Johnson, C. K.; Greig, D. J.; Kramer, S.; Che, X.; Wells, H.; Hicks, A. L.; Joly, D. O.; Wolfe, N. D.; Daszak, P.; Karesh, W.; Lipkin, W. I.; Morse, S. S.; Mazet, J. A. K.; Goldstein, T. Global patterns in coronavirus diversity. Virus Evol 2017, 3 (1), vex012
7. Lu, R.; Zhao, X.; Li, J.; Niu, P.; Yang, B.; Wu, H.; Wang, W.; Song, H.; Huang, B.; Zhu, N.; Bi, Y.; Ma, X.; Zhan, F.; Wang, L.; Hu, T.; Zhou, H.; Hu, Z.; Zhou, W.; Zhao, L.; Chen, J.; Meng, Y.; Wang, J.; Lin, Y.; Yuan, J.; Xie, Z.; Ma, J.; Liu, W. J; Wang, D.; Xu, W.; Holmes, E. C; Gao, G. F; Wu, G.; Chen, W.; Shi, W.; Tan, W. Genomic characterization and epidemiology of 2019 novel coronavirus: implications for virus origins and receptor binding. Lancet 2020, 395, 565-574.
8. Shang, Jian, et al. "Structural basis of receptor recognition by SARS-CoV-2." *Nature* (2020): 1-4.
9. Yan, Renhong, et al. "Structural basis for the recognition of SARS-CoV-2 by full-length human ACE2." *Science* 367.6485 (2020): 1444-1448.

10. Dong, N., et al. Genomic and protein structure modelling analysis depicts the origin and infectivity of 2019-nCoV, a new coronavirus which caused a pneumonia outbreak in Wuhan, China, bioRxiv 2020, DOI: 10.1101/2020.01.20.913368
11. Wrapp, D.; Wang, N.; Corbett, K. S.; Goldsmith, J. A.; Hsieh, C.-L.; Abiona, O.; Graham, B. S.; McLellan, J. S. Cryo-EM structure of the 2019-nCoV Spike in the prefusion conformation. Science 2020, eabb2507.
12. Hoffmann, M.; Kleine-Weber, H.; Schroeder, S.; Kruger, N.; Herrler, T.; Erichsen, S.; Schiergens, T. S.; Herrler, G.; Wu, N.-H.; Nitsche, A.; Muller, M. A.; Drosten, C.; Pohlmann, S. SARS-CoV-2 Cell Entry Depends on HACE-2 and TMPRSS2 and Is Blocked by a Clinically Proven Protease Inhibitor. Cell 2020, DOI: 10.1016/ j. cell.2020.02.052. [Epub ahead of print].
13. Gorbalenya, A. E.; Snijder, E. J.; Ziebuhr, J. Virus-encoded proteinases and proteolytic processing in the Nidovirales. J. Gen. Virol. 2000, 81 (4), 853-879
14. Baez-Santos, Y. M.; St. John, S. E.; Mesecar, A. D. The SARS coronavirus papain-like protease: structure, function and inhibition by designed antiviral compounds. Antiviral Res. 2015, 115, 21-38.
15. Zhou, P. et al. A pneumonia outbreak associated with a new coronavirus of probable bat origin. Nature 579, 270–273 (2020).
16. 2. Wu, F. et al. A new coronavirus associated with human respiratory disease in China. Nature 579, 265–269 (2020).
17. 3. Zhu, N. et al. A novel coronavirus from patients with pneumonia in China, 2019. N. Engl. J. Med. 382, 727–733 (2020).
18. Lee, T.-W.; Cherney, M. M.; Huitema, C.; Liu, J.; James, K. E.; Powers, J. C.; Eltis, L. D.; James, M. N.G. Crystal structures of the main peptidase from the SARS coronavirus inhibited by a substrate like aza-peptide epoxide. J. Mol. Biol. 2005, 353 (5), 1137-1151
19. Lan, J., Ge, J., Yu, J., Shan, S., Zhou, H., Fan, S., ... & Wang, X. (2020). Structure of the SARS-CoV-2 spike receptor-binding domain bound to the ACE2 receptor. *Nature*, 1-6.
20. Zhang, G., Pomplun, S., Loftis, A. R., Loas, A., & Pentelute, B. L. The first-in-class peptide binder to the SARS-CoV-2 spike protein. bioRxiv. *Doi*, *10*(2020.03), 19-999318.
21. Han, Y., & Král, P. (2020). Computational Design of ACE2-Based Peptide Inhibitors of SARS-CoV-2. ACS nano.

22. Van Zundert, G. C. P., Rodrigues, J. P. G. L. M., Trellet, M., Schmitz, C., Kastritis, P. L., Karaca, E., ... & Bonvin, A. M. J. J. (2016). The HADDOCK2. 2 web servers: user-friendly integrative modeling of biomolecular complexes. Journal of molecular biology, 428(4), 720-725.
23. Gurtovenko, A. A., & Vattulainen, I. (2005). Pore formation coupled to ion transport through lipid membranes as induced by transmembrane ionic charge imbalance: atomistic molecular dynamics study. *Journal of the American Chemical Society*, *127*(50), 17570-17571.
24. Van Der Spoel, D., Lindahl, E., Hess, B., Groenhof, G., Mark, A. E., & Berendsen, H. J. (2005). GROMACS: fast, flexible, and free. *Journal of computational chemistry*, *26*(16), 1701-1718.
25. Singh, Vishal K., et al. "Anti-HIV potential of diarylpyrimidine derivatives as non-nucleoside reverse transcriptase inhibitors: Design, synthesis, docking, TOPKAT analysis and molecular dynamics simulations." *Journal of Biomolecular Structure and Dynamics* (2020): 1-17.
26. Sen Gupta, Parth Sarthi, et al. "Screening and molecular characterization of lethal mutations of human homogentisate 1, 2 dioxigenase." *Journal of Biomolecular Structure and Dynamics* (2020): 1-11.
27. Kumari et al (2014) g_mmpbsa - A GROMACS tool for high-throughput MM-PBSA calculations. *J. Chem. Inf. Model.* 54:1951-1962.
28. Baker *et al.* (2001) Electrostatics of nanosystems: Application to microtubules and the ribosome. *Proc. Natl. Acad. Sci. USA* 98:10037-10041.

Supporting Information

Table S1: The contribution (in kJ/mol) of each residue present in α-1 helix and the designed peptide inhibitor 13 to binding to the spike protein.

Residue no.	α-1 helix	Residue no.	Peptide inhibitor 13
I21	17.45	I21	22.69
E22	-15.10	D22	-19.37
E23	-13.92	W23	-5.72
Q24	0.00	Q24	-0.081
A25	-0.21	F25	-0.49
K26	19.09	W26	-8.05
T27	-2.06	F27	-2.22
F28	-3.00	H28	-0.50
L29	-0.18	Y29	-0.53
D30	-20.04	D30	-18.19
K31	19.88	K31	27.67
F32	-0.42	W32	-2.09
N33	0.30	D33	-10.87
H34	-1.48	H34	-1.09
E35	-15.15	E35	-23.39
A36	0.10	W36	-2.43
E37	-22.27	E37	-27.06

D38	-20.17	D38	-21.96
L39	-0.17	E39	-21.66
F40	-0.06	W40	-6.93
Y41	-1.30	Y41	-0.70
Q42	0.50	Q42	1.03
S43	0.46	S43	0.25
S43	-20.49	S44	-16.17